Numerical Methods in Civil Engineering, 5-4 (2021) 46-59

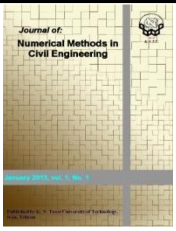

Numerical Methods in Civil Engineering

Journal Homepage: https://nmce.kntu.ac.ir/

Analyzing of thick plates with cutouts using the meshless (EFG) method based on higher order shear deformation theories for solving shear-locking issue

Seyed Amin Vakili*, Farzad Shahabian, and Mohammad Hossein Ghadiri Rad*****

ARTICLE INFO

RESEARCH PAPER

Article history:
Received:
February 2021.
Revised:
April 2021.
Accepted:
May 2021.

Keywords:
EFG method,
Thick plate,
Cutout,
Shear locking
Higher-order shear deformation theories

Abstract:

Although the finite element method (FEM) is a well-established method for modelling the thick plates, in some cases FEM encounters some difficulties such as shear locking and decrease in the accuracy of results caused by stress concentration around the openings. In this paper for the first time, the EFG method based on the higher-order shear deformation theories is developed for analysis of thick plates with cutout to overcome these drawbacks. It should be mentioned that the EFG method does not need any mesh generation in problem domain and its boundaries. The Radial Point Interpolation method (RPIM) is used to discrete the problem domain. Several numerical examples are analyzed using proposed method and effects of aspect ratios, boundary conditions and location of cutout are discussed in details. Results show that by choosing the appropriate shape functions for the deflection and rotations, the presented EFG method has successfully overcome the shear-locking problem. Based on numerical results, the best position of circular cutout, which minimizes the maximum deflection is determined. The approximate equations for determination of maximum deflection are presented using the cubic polynomial method. Numerical implementations show that the presented method has high efficiency, good accuracy and easy implementation.

1. Introduction

In recent decades, thick plates have had various utilizations in retaining walls, rehabilitation of damaged structures, aerospace industry, marine structures and nuclear industry. Since the analytical solution of plates is limited to simple geometry and boundary conditions, a variety of numerical methods such as finite element have been proposed for analysis of plates with complex geometry and boundary conditions [1, 2]. In spite of the effective application of finite element method in many problems, this method has inherent shortcomings such as high cost in creating mesh, difficulty in adaptive analysis, requirement to predefined mesh, formation of shear lock phenomenon in higher order shear deformation and mesh complexity issue in plate with discontinuity in the domain. Hence, in recent years, the meshless methods have attracted significant attention of researchers [3, 4].

* *Ph.D. Student, Department of Civil Engineering, Faculty of Engineering, Ferdowsi University of Mashhad, Mashhad, Iran.*
** *Corresponding Author: Professor, Department of Civil Engineering, Faculty of Engineering, Ferdowsi University of Mashhad, Mashhad, Iran; E-mail: shahabf@um.ac.ir*
*** *Assistant Professor, Department of Civil Engineering, Quchan University of Technology, Quchan, Iran.*

The meshless methods have been developed and applied in many engineering problems, especially in structural analysis including beams, plates and shells since the middle of 1990s. Meshless is a method used to establish system algebraic equations for the whole problem domain without the use of a predefined mesh for the domain discretization. The ideal feature for this technique is that, no mesh is required throughout the process of formulating and solving the problem of a given arbitrary geometry governed by partial differential system equations subject to boundary conditions [5, 6]. In this method, the discretization of the domain of the problem takes place using nodal points, and the shape function of each node is defined using the nodal points of the domain covered by that node. This feature allows for a more accurate solution to the issues of discontinuity in the domain, such as the cutout, cracks and corrosion in thick plates.

Meshless methods can be roughly divided into three groups namely; strong form, weak form and the last one is associated with weak and strong ones of system equations [5, 7]. The strong forms are directly implemented from governing differential equations consisting of the general finite difference method [8,9], the smooth particle hydrodynamic method [10] and the meshless collocation method [11]. The weak form includes the element-free Galerkin (EFG) method [12], the reproducing kernel particle method [13,14], the meshless local Petrov–Galerkin method [15], the radial point interpolation method (RPIM) [5,16,17] and the moving Kriging interpolation (MKI) method [18,19]. The last one which is mostly considered, is the meshless weak–strong form (MWS) method [20, 21]. Meshless methods based on the Galerkin weak form require a background mesh to compute the quadrature integrations [22-24]. Generally speaking, meshless shape functions are rational and hence the higher-order quadrature needs to be employed to achieve stable and accurate solutions, however, computation cost is very expensive. The lower order quadrature retains less CPU times but the solutions cannot be converged and stabilized [25,26]. The nodal integration technique is found to be an appropriate choice.

Sladek et al. [27] presented a new meshless method to solve bending problems of thin elastic plates with large deflections but, contrary to the conventional boundary integral equation method all integrals in the present formulation are regular and no special computational techniques are required to evaluate the integrals. Alihemmati et al. [28] developed the 3D meshless Galerkin method for structural analysis of general polygonal geometries. They showed this method can cover the plates with considerable thickness, that the classical plate theories cannot solve them with accurate results. Cao et al. [29] compared the results of meshless method with coupled FEM-EFG and coupled BEM-EFG methods. Choi et al [30] presented the analysis of Mindlin plate by the EFG procedure-applying penalty (EFGMP) technique. They showed the EFGMP is much more accurate than FEM for Mindlin plate even when linear basis functions are used.

Donning et al. [31] proposed the meshless method for shear-deformable beams and plates. They used this method to eliminate shear and membrane locking in beams and plates using an unmodified displacement-based vibrational principle. Gulizzi et al. [32] presented an implicit mesh discontinuous Galerkin formulation for higher-order shear deformation plate theories. Khezri et al. [33] presented a unified approach to meshless analysis of thin to moderately thick plates based on a shear-locking-free Mindlin theory. They extended the modified Mindlin formulation so as to completely suppress shear-locking effects. Konda et al. [34] proposed a meshless Reissner plate bending procedure using local radial point interpolation with an efficient integration scheme. Li, Y et al. [35] presented an element-free smoothed radial point interpolation method (EFS-RPIM) for 2D and 3D solid mechanics problems. Liu, X et al. [36] suggested a wavelet multiresolution interpolation Galerkin method. Rad et al. [37] developed the meshless local Petrov–Galerkin method for nonlinear dynamic analyses of hyper-elastic FG thick hollow cylinder with Rayleigh damping. They demonstrated that when the cylinder is thick enough, the results of nonlinear analysis are close to the results of linear ones. Thai et al. [38] investigated a moving Kriging interpolation meshless method based on naturally stabilized nodal integration scheme for plate analysis. They showed the complexity of the heterogeneous structure could be treated via the concept of homogenization. Thai, H. T et al. [39] developed an analytical solution for refined plate. Ferreira et al. [40] presented a meshless strategy using the Generalized Finite Difference Method (GFDM) for plate bending problems. They showed that by using this method, the original fourth-order differential equation could be substituted by a system composed of two second-order partial differential equations.

In this paper, the EFG method is developed to analyze thick plates with and without cutout. It should be mentioned that the EFG method is one of the most popular meshless methods because of its similarities with FEM. This technique is based on global weak form of governing differential equation. Though there exists a background cell for integration, there is no need to refine the integration cell when decreasing nodal distance for more accurate field approximation. Thus, the EFG method has high convergence rate and the computational time required for this method is less than other meshless methods. The radial basis functions with Kronecker delta function are used as the shape functions. The first and third deformation theories are implemented in analysis of thick plates. Effects of plate dimensions, boundary conditions and location of circular cutout on maximum transverse displacement of plates are determined by several numerical examples. Finally, interpolation equations for determination of maximum deflection of plates with and without cutouts are presented using the cubic polynomial method.

2. Fundamental equations of thick plates

In higher order shear deformation theories of first order shear deformation theory (FSDT) and third order shear deformation theory (TSDT), in contrast with the Classical Plate Theory (CPT) method the transverse shear strains are considered using the first and third functions in thickness direction [41,42]. Actually, the FSDT develops the kinematics of the CPT by relaxing the normality restriction and authority for arbitrary but constant rotation of transverse normal [42,43]. The FSDT formulation is very similar to that of the Timoshenko beam, but is extended in one more dimension. The TSDT subsequent the kinematics hypothesis by eliminating the transverse normal straightness hypothesis; i.e., the straight normal to the middle plane before deformation develops into cubic curves after deformation (See Fig. 1) [34, 44]. Considering a thick plate element as shown in Fig. 2, it is assumed that the vertical load perpendicular to the plate is only resisted by flexure and shear stresses (i.e., $\sigma_{zz} \approx 0$).

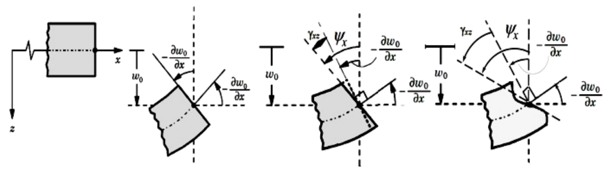

(a) CPT **(b) FSDT** **(c) TSDT**

Fig. 1: Deformation of a transverse normal to the middle plane with different plate theories [42]

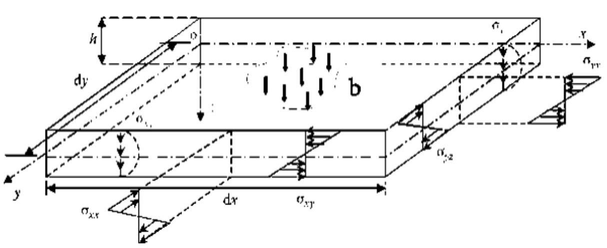

Fig. 2: Stresses representation

Therefore, the non-zero stresses can be expressed by [33, 45]:

$$\underbrace{\begin{Bmatrix} \sigma_{xx} \\ \sigma_{yy} \\ \sigma_{xy} \\ \sigma_{xz} \\ \sigma_{yz} \end{Bmatrix}}_{} = \underbrace{\frac{E}{1-\nu^2} \cdot \begin{bmatrix} 1 & \nu & 0 & 0 & 0 \\ \nu & 1 & 0 & 0 & 0 \\ 0 & 0 & \frac{1-\nu}{2} & 0 & 0 \\ 0 & 0 & 0 & \Theta.\frac{1-\nu}{2} & 0 \\ 0 & 0 & 0 & 0 & \Theta.\frac{1-\nu}{2} \end{bmatrix}}_{D} \underbrace{\begin{Bmatrix} \varepsilon_{xx} \\ \varepsilon_{yy} \\ \gamma_{xy} \\ \gamma_{xz} \\ \gamma_{yz} \end{Bmatrix}}_{\varepsilon} = D.\varepsilon \tag{1}$$

where ν is the Poissons ratio, E is the Youngs modulus, D is the flexural rigidity of the plate, Θ is the shear correction factor for thick plates that can be expressed by the following equation [33]:

$$\Theta = \frac{20(1+\nu)}{24+25\nu+\nu^2} \xrightarrow{\nu=0.3} \Theta \cong \frac{5}{6} \tag{2}$$

2.1. FSDT formulation for thick plate

According to the FSDT theory, the in-plane displacements u, v which are parallel to the unformed neutral surface, can be expressed by [42,43]:

$$\begin{aligned} u(x,y,z) &= z\psi_x(x,y) \\ v(x,y,z) &= z\psi_y(x,y) \\ w(x,y,z) &= w_0(x,y) \end{aligned} \tag{3}$$

$$\frac{\partial u}{\partial z} = \psi_x \qquad \frac{\partial v}{\partial z} = \psi_y \tag{4}$$

where w_0 represents the transverse displacements of a point on the middle plane $\mathrm{z}=0$, ψ_x and ψ_y are rotations of a transverse normal about the y and x axes, respectively. Using the FSDT formulation, the displacements introduced in Eq. (5) can be expressed in following matrix form:

$$\underbrace{\begin{Bmatrix} u \\ v \\ w \end{Bmatrix}}_{\hat{U}} = \underbrace{\begin{bmatrix} 0 & z & 0 \\ 0 & 0 & z \\ 1 & 0 & 0 \end{bmatrix}}_{L_u} \underbrace{\begin{Bmatrix} w_0 \\ \psi_x \\ \psi_y \end{Bmatrix}}_{U} = L_u.U \tag{5}$$

Thus, the strain vector of the thick plate can be expressed with respect to the displacement vector as [2]:

$$\underbrace{\begin{Bmatrix} \varepsilon_{xx} \\ \varepsilon_{yy} \\ \varepsilon_{xy} \\ \varepsilon_{xz} \\ \varepsilon_{yz} \end{Bmatrix}}_{\varepsilon} = \underbrace{\begin{bmatrix} 0 & 0 & 0 & \frac{\partial}{\partial x} & \frac{\partial}{\partial y} \\ z\frac{\partial}{\partial x} & 0 & z\frac{\partial}{\partial y} & 1 & 0 \\ 0 & z\frac{\partial}{\partial y} & z\frac{\partial}{\partial x} & 0 & 1 \end{bmatrix}}_{L_d^T} \begin{Bmatrix} w_0 \\ \psi_x \\ \psi_y \end{Bmatrix} = L^T{}_d.U \tag{6}$$

2.2. TSDT formulation for thick plate

In order to achieve higher accuracy and eliminate shear correction coefficients in FSDT, the TSDT is recommended. In this method, variation of the transverse shear strains and transverse shear stresses through the plate thickness are considered using third order functions. According to the TSDT, the kinematic hypothesis is further relaxed by eliminating the straightness hypothesis; i.e., straight normal to the middle plane before deformation may emerge as cubic curves after deformation (See Fig. 1(c)). Therefore, similar to the FSDT (Section 2.1), the displacement field of the thick plate can be expressed by [42]:

$$\begin{aligned} u(x,y,z) &= z\psi_x(x,y) - \chi\left(\psi_x + \frac{\partial w_0}{\partial x}\right) \\ v(x,y,z) &= z\psi_y(x,y) - \chi\left(\psi_y + \frac{\partial w_0}{\partial y}\right) \qquad \textit{where} \quad \chi = \frac{4z^3}{3h^2} \\ w(x,y,z) &= w_0(x,y) \end{aligned} \tag{7}$$

According to the above equation, the displacement vector can be expressed in the following matrix form [2]:

$$\underbrace{\begin{Bmatrix} u \\ v \\ w \end{Bmatrix}}_{\hat{U}} = \underbrace{\begin{bmatrix} -\chi z^3\frac{\partial}{\partial x} & z-\chi z^3 & 0 \\ -\chi z^3\frac{\partial}{\partial y} & 0 & z-\chi z^3 \\ 1 & 0 & 0 \end{bmatrix}}_{L_u} \underbrace{\begin{Bmatrix} w_0 \\ \psi_x \\ \psi_y \end{Bmatrix}}_{U} = L_u U \tag{8}$$

In TSDT formulation using the general strain–displacement relationship, the strains of thick plates can be expressed by [2]:

$$\underbrace{\begin{Bmatrix} \varepsilon_{xx} \\ \varepsilon_{yy} \\ \varepsilon_{xy} \\ \varepsilon_{xz} \\ \varepsilon_{yz} \end{Bmatrix}}_{\varepsilon} = \underbrace{\begin{bmatrix} -\chi z^3 \dfrac{\partial^2}{\partial x^2} & \left(z-\chi z^3\right)\dfrac{\partial}{\partial x} & 0 \\ -\chi z^3 \dfrac{\partial^2}{\partial y^2} & 0 & \left(z-\chi z^3\right)\dfrac{\partial}{\partial y} \\ -\chi z^3 \dfrac{\partial^2}{\partial x \partial y} & \left(z-\chi z^3\right)\dfrac{\partial}{\partial y} & \left(z-\chi z^3\right)\dfrac{\partial}{\partial x} \\ \left(1-\eta . z^2\right)\dfrac{\partial}{\partial x} & \left(1-\eta z^2\right) & 0 \\ \left(1-\eta . z^2\right)\dfrac{\partial}{\partial y} & 0 & \left(1-\eta z^2\right) \end{bmatrix}}_{L_d} \underbrace{\begin{Bmatrix} w_0 \\ \psi_x \\ \psi_y \end{Bmatrix}}_{U} = L_d U \qquad where \quad \eta = 3\chi \tag{9}$$

2.3. Essential Boundary Conditions

The essential boundary conditions of thick plates associated with the free and clamped outer edges can be defined as:

Free (simply supported) edges: $w_0\big|_{at\,edage} = 0$ (10)

Fixed (clamped) edges:

$$w_0\big|_{at\,edage} = 0 \qquad \psi_t\big|_{at\,edage} = 0 \qquad \psi_n\big|_{at\,edage} = 0 \tag{11}$$

where ψ_t and ψ_n are rotations with respect to the axes of perpendicular to the tangent and normal direction to the boundary, respectively.

3. Shape function with radial point interpolation method

The major drawback of polynomial interpolation method (PIM) is the singularity of moment matrix in some cases [2]. To create a nonsingular moment matrix, the Radial basis function (RBF) is used to develop the RPIM shape functions [2,5]. Consider a function u(x) defined in the problem domain Ω. The RPIM interpolates $U(x)$ using the nodal values at the nodes located in support domain of a point of interest x_Q. The RPIM formulation starts with the following finite series representation [2]:

$$U^h(x, x_Q) = \sum_{i=1}^{n} R_i(x,y)\, a_i(x_Q) = R^T a(x_Q) \tag{12}$$

where n is the number of nodes in the support domain of point x_Q, $a_i(x_Q)$ is the coefficient vector and $R_i(x,y)$ is the radial basis functions. These parameters can be expressed as:

$$\{a(x_Q)\}^{\mathrm{T}} = \{a_1 \;\; a_2 \;\; \ldots \;\; a_n\} \qquad R^T = [R_1(x,y), R_2(x,y), \ldots, R_n(x,y)] \tag{13}$$

$$R_i(x,y) = \left(r_i^2 + C^2\right)^q \quad r_i = \sqrt{(x-x_i)^2 + (y-y_i)^2} \quad C = \alpha_C . d_C \quad where \;\; q \cong 1.03 \;\; \alpha_C = 1 \tag{14}$$

where r_i is the distance between the sampling point x_i and node x_Q, α_c is the dimensionless shape parameter, d_c is the characteristic length which is the average nodal spacing for all the n nodes located in the support domain. The vector that collects the values of field variables at all the `n` nodes in the support domain $\overline{U}$ can be expressed as:

$$\overline{U} = \left\{U_1 \;\; U_2 \;\; \ldots \;\; U_i\Big|_{i=1}^{n}\right\}^T = \left\{w_{01}\,\psi_{x1}\,\psi_{y1} \;\; w_{02}\,\psi_{x2}\,\psi_{y2} \;\; \ldots\ldots \;\; w_{0i}\,\psi_{xi}\,\psi_{yi}\Big|_{i=1}^{n}\right\}^T \tag{15}$$

Using Eq. (12), the coefficient vector can be calculated by:

$$\overline{U} = R_Q\, a \rightarrow a = R_Q^{-1}\overline{U} \tag{16}$$

where R_Q is the moment matrix of RBF:

$$R_Q = \begin{bmatrix} R_1(r_1) & R_2(r_1) & \cdots & R_n(r_1) \\ R_1(r_2) & R_2(r_2) & \cdots & R_n(r_2) \\ \vdots & \vdots & \ddots & \vdots \\ R_1(r_n) & R_2(r_n) & \cdots & R_n(r_n) \end{bmatrix}_{(n \times n)} \tag{17}$$

Substituting the Eqs. (16) and (17) into Eq. (12), can be written as:

$$U^h(x,y) = \underbrace{R^T(x,y) R_Q^{-1}}_{\overline{\Phi}(x,y)}\overline{U} = \overline{\Phi}(x,y)\overline{U} = \{\Phi_1(x,y) \quad \Phi_2(x,y) \quad \Phi_3(x,y) \ldots\ldots \Phi_n(x,y)\}\overline{U} \tag{18}$$

In which $\Phi_i(x,y)$ is the shape function for the *i*-th node. Finally, the RPIM shape functions corresponding to transverse displacement and rotations of the *i*-th node can be obtained as follows:

$$\Phi_i(x,y) = \begin{bmatrix} \hat{\Phi}_i(x,y) & 0 & 0 \\ 0 & \hat{\Phi}_{i,x}(x,y) & 0 \\ 0 & 0 & \hat{\Phi}_{i,y}(x,y) \end{bmatrix} \tag{19}$$

where $\hat{\Phi}_i$ is the shape function for w_0 and $\Phi_{i,x}$, $\hat{\Phi}_{i,y}$ are derivatives of the shape function for the two field variables ψ_x, ψ_y respectively Substituting the Eq. (19) into Eq. (18), one can write:

$$U^h(x) = \overline{\Phi}(x,y)\overline{U} = \sum_{i=1}^{n} \Phi_i(x,y) U_i = \sum_{i=1}^{n} \begin{bmatrix} \hat{\Phi}_i(x,y) & 0 & 0 \\ 0 & \hat{\Phi}_{i,x}(x,y) & 0 \\ 0 & 0 & \hat{\Phi}_{i,y}(x,y) \end{bmatrix} \begin{Bmatrix} w_{0i} \\ \Psi_{xi} \\ \Psi_{yi} \end{Bmatrix} \tag{20}$$

Note; for elimination of shear locking, the shape functions for the rotations ψ_x and ψ_y are produced from the first-order derivatives of the shape function used for the transverse displacement w_0 [2]. The derivative of shape functions $\hat{\Phi}_{i,x}, \hat{\Phi}_{i,y}$ are introduced in the Appendix A.

4. EFG method for thick plates with cutout

Consider the domain $\Omega\big|_{\tilde{\Omega}-\Omega_{Cutout}}$ bounded by $\Gamma = \Gamma^u_{Cutout} \cup \Gamma_u \cup \Gamma_t$ where Γ_u denotes the essential boundary and Γ_t denotes the traction boundaries. The superscripts (s) and (e) are used to side and edge surfaces of the traction boundaries (See Fig. 3).

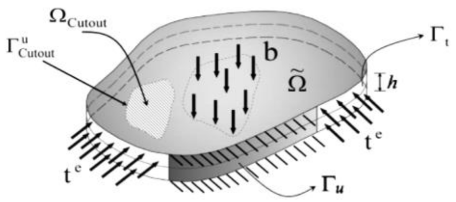

Fig. 3: Schematic view of thick plate subjected to transverse loads and thickness h

Although the RPIM shape function has the Kronecker delta property, for clamed supports, in which the both edge deflection and edge slopes should be equal to zero, the use of Lagrange multipliers method is inevitable. The Galerkin weak form with Lagrange multipliers for constraints is given by [2]:

$$\int_{\Omega} \delta\left((L_d U^h)^T D\left(L_d U^h\right)\right) d\Omega - \int_{\Omega} (\delta U^h)^T b\, d\Omega - \int_{\Gamma_t} (\delta U^h)^T t^e d\Gamma_t - \int_{\Gamma u} \delta\lambda^T\left(U^h - u_\Gamma\right) d\Gamma - \int_{\Gamma u} \delta U^{h^T} \lambda\, d\Gamma = 0 \tag{21}$$

where b is the vector of external body forces, u_Γ is the prescribed displacement on the essential (displacement) boundaries Γ_u and U^h is the displacement vector given by Eq. (20). The last two terms in Eq. (21) are produced by the method of Lagrange multipliers for handling essential boundary conditions for cases when $U^h - u_\Gamma \neq 0$. The Lagrange multipliers λ here can be viewed physically as smart forces that can force $U^h - u_\Gamma = 0$. In Eq. (21), the compatible strain $L_d U^h$ for FSDT and TSDT formulations can be expressed as:

FSDT:

$$L_d U^h = L_d \sum_{i=1}^{n} \Phi_i U_i = \underbrace{\sum_{i=1}^{n} \begin{bmatrix} 0 & z\frac{\partial}{\partial x} & 0 \\ 0 & 0 & z\frac{\partial}{\partial y} \\ 0 & z\frac{\partial}{\partial y} & z\frac{\partial}{\partial x} \\ \frac{\partial}{\partial x} & 1 & 0 \\ \frac{\partial}{\partial y} & 0 & 1 \end{bmatrix} \begin{bmatrix} \hat{\Phi}_i(x,y) & 0 & 0 \\ 0 & \hat{\Phi}_{i,x}(x,y) & 0 \\ 0 & 0 & \hat{\Phi}_{i,y}(x,y) \end{bmatrix}}_{\sum_{i=1}^{n}(B_F)} \begin{Bmatrix} w_{0i} \\ \Psi_{xi} \\ \Psi_{yi} \end{Bmatrix} = \sum_{i=1}^{n} (B_F)_i U_i \tag{22}$$

TSDT:

$$L_d U^h = \underbrace{\sum_{i=1}^{n} \begin{bmatrix} -\chi z^3 \frac{\partial^2}{\partial x^2} & \left(z - \chi z^3\right)\frac{\partial}{\partial x} & 0 \\ -\chi z^3 \frac{\partial^2}{\partial y^2} & 0 & \left(z - \chi z^3\right)\frac{\partial}{\partial y} \\ -\chi z^3 \frac{\partial^2}{\partial x \partial y} & \left(z - \chi z^3\right)\frac{\partial}{\partial y} & \left(z - \chi z^3\right)\frac{\partial}{\partial x} \\ \left(1 - \eta . z^2\right)\frac{\partial}{\partial x} & \left(1 - \eta z^2\right) & 0 \\ \left(1 - \eta . z^2\right)\frac{\partial}{\partial y} & 0 & \left(1 - \eta z^2\right) \end{bmatrix} \begin{bmatrix} \hat{\Phi}_i(x,y) & 0 & 0 \\ 0 & \hat{\Phi}_{i,x}(x,y) & 0 \\ 0 & 0 & \hat{\Phi}_{i,y}(x,y) \end{bmatrix}}_{\sum_{i=1}^{n}(B_T)} \begin{Bmatrix} w_{0i} \\ \Psi_{xi} \\ \Psi_{yi} \end{Bmatrix} = .. \tag{23}$$

$$= \sum_{i=1}^{n} (B_F)_i U_i$$

Note that the second derivatives of shape functions $\hat{\Phi}_{i,xx}, \hat{\Phi}_{i,yy}, \hat{\Phi}_{i,xy}$ are introduced in the appendix A. The Lagrange multiplier vector λ in Eq. (21) is an unknown function of the coordinates, which needs also to be treated as a field variable and interpolated using the nodes on the essential boundaries to obtain a set of discrete system equations:

$$\lambda(\hat{x}) = \sum_{i \in S_\lambda} \tilde{N}_i(s)\lambda_i \qquad \hat{x} \in \Gamma_u \tag{24}$$

where: S_λ is the set of nodes used for this interpolation

s is the curvilinear coordinate along the essential boundary

λ_i is the Lagrange multiplier at node i on the essential boundary.

$\tilde{N}_i(s)$ is the Lagrange interpolant of order r which can be given in general as follows:

$$\tilde{N}_k^r(s) = \prod_{\substack{i=0 \\ i \neq k}}^{r} \frac{(s - s_i)}{(s_k - s_i)} \tag{25}$$

The vector of Lagrange multipliers in Eq. (21) can be written in the matrix form:

$$\lambda = \sum_{i \in S_\lambda} \underbrace{\begin{bmatrix} \tilde{N}_i & 0 & 0 \\ 0 & \tilde{N}_i & 0 \\ 0 & 0 & \tilde{N}_i \end{bmatrix}}_{\overline{\mathrm{N}}_i} \underbrace{\begin{Bmatrix} \lambda_{w0i} \\ \lambda_{\psi xi} \\ \lambda_{\psi yi} \end{Bmatrix}}_{\lambda_i} = \sum_{i \in \delta_\lambda} \overline{\mathrm{N}}_i \lambda_i \tag{26}$$

Substituting Eqs. (22) and (23) into Eq. (24), one can write:

$$\int_{\Omega} \delta\left(\sum_{i \in S_n} B_i U_i\right)^T \left(D \sum_{j \in S_n} B_j U_j\right) d\Omega - \int_{\Omega} \delta\left(\sum_{i \in S_n} \Phi_i U_i\right)^T b\, d\Omega - \int_{\Gamma_t} \delta\left(\sum_{i \in S_n} \Phi_i U_i\right)^T t^e d\Gamma - .... \tag{27}$$

$$- \int_{\Gamma_u} \delta\lambda^T \left(\left(\sum_{i \in S_n} \Phi_i U_i\right) - u_\Gamma\right) d\Gamma - \int_{\Gamma_u} \delta\left(\sum_{i \in S_n} \Phi_i U_i\right)^T \lambda\, d\Gamma = 0$$

where for FSDT $B_i = (B_F)_i$, $B_j = (B_F)_j$ and TSDT $B_i = (B_T)_i$, $B_j = (B_T)_j$. In the first integral term, we have:

$$\int_{\Omega} \delta\left(\sum_{i \in S_n} B_i U_i\right)^T \left(D \sum_{j \in S_n} B_j U_j\right) d\Omega = \int_{\Omega} \delta\left(\sum_{i \in S_n} U_i^T B_i^T\right)\left(D \sum_{j \in S_n} B_j U_j\right) d\Omega \to ...$$

$$\int_{\Omega} \delta\left(\sum_{i \in S_n} U_i^T B_i^T\right)\left(D \sum_{j \in S_n} B_j U_j\right) d\Omega = \sum_{i \in S_n} \sum_{j \in S_n} \delta U_i^T \underbrace{\int_{\Omega} B_i^T D B_j d\Omega}_{K_{ij}} U_j = \sum_{i \in S_n} \sum_{j \in S_n} \delta U_i^T K_{ij} U_j \tag{28}$$

$$K_{ij} = \int_{\Omega} B_i^T D B_j d\Omega \tag{29}$$

The stiffness coefficients K_{ij} is listed in the Appendix B.

The second term in Eq. (28) can be expressed as:

$$\int_{\Omega} \delta\left(\sum_{i \in S_n} \Phi_i U_i\right)^T b\, d\Omega = \sum_{i \in S_n} \delta U_i^T \underbrace{\int_{\Omega} (\Phi_i)^T b\, d\Omega}_{f_i} = \sum_{i \in S_n} \delta U_i^T f_i = \delta \overline{U}^T \overline{F}_\Omega \tag{30}$$

where f_i is called the nodal force vector and $\overline{F}_\Omega$ is all of node force vectors on Ω domain. The additional nodal force vector can be given as:

$$f_i = \int_{\Gamma_t} (\Phi_i)^T t^e d\Gamma \tag{31}$$

Finally:

$$F_I = \int_{\Omega} (\Phi_i)^T b\, d\Omega + \int_{\Gamma_t} (\Phi_i)^T t^e d\Gamma \tag{32}$$

Since in this paper the membrane forces are neglected, the amount of t^e is zero. The last term in Eq. (21) is:

$$\int_{\Gamma_u} \delta\left(\sum_{i\in S_n} \Phi_i U_i\right)^T \lambda d\Gamma = \int_{\Gamma_u} \delta\left(\sum_{i\in S_n} \Phi_i U_i\right)^T \left(\sum_{j\in S_n} \bar{N}_j \lambda_j\right) d\Gamma = \sum_{i\in S_n}\sum_{j\in S_\lambda} \delta U_i^T \underbrace{\int_{\Gamma_u} (\Phi_i)^T \bar{N}_j d\Gamma}_{-G_{ij}} \lambda_j = \dots \tag{33}$$

$$\dots - \sum_{i\in S_n}^{n}\sum_{j\in S_n}^{n\lambda_t} \delta U_i^T G_{ij} \lambda_j = -\delta U^T G\lambda$$

$$G_{ij} = -\int_{\Gamma_u} (\Phi_i)^T \mathrm{N}_j d\Gamma \tag{34}$$

where $n\lambda_t$ is the total number of nodes on the essential boundary and G is also a global matrix formed by assembling its nodal matrix G_{ij}. Finally:

$$\underbrace{\int_{\Omega} \delta\left(\sum_{i\in S_n} (B)_i U_i\right)^T \left(D \sum_{j\in S_n} (B)_j U_j\right) d\Omega}_{\delta U^T KU} - \underbrace{\int_{\Omega} \delta\left(\sum_{i\in S_n} \Phi_i U_i\right)^T b d\Omega - \int_{\Gamma_t} \delta\left(\sum_{i\in \delta_n} \Phi_i U_i\right)^T t^e d\Gamma}_{\delta U^T F} \dots$$

$$- \underbrace{\int_{\Gamma_u} \delta\lambda^T \left(\left(\sum_{i\in S_n} \Phi_i U_i\right) - u_\Gamma\right) d\Gamma}_{\delta\lambda^T \left[G^T U - q\right]} - \underbrace{\int_{\Gamma_u} \delta\left(\sum_{i\in S_n} \Phi_i U_i\right)^T \lambda d\Gamma}_{\delta U^T G\lambda} = 0 \tag{35}$$

where the vector q_i can be expressed as:

$$q_i = -\int_{\Gamma u} \bar{\mathrm{N}}_i^T u_\Gamma d\Gamma \tag{36}$$

which is:

$$\delta U^T\left[KU + G\lambda - F\right] + \delta\lambda^T\left[G^T U - q\right] = 0 \tag{37}$$

Because ∂U and $\partial\lambda$ are arbitrary, the above equation can be satisfied only if:

$$\begin{bmatrix} K & G \\ G^T & 0 \end{bmatrix} \begin{Bmatrix} U \\ \lambda \end{Bmatrix} = \begin{Bmatrix} F \\ q \end{Bmatrix} \tag{38}$$

This is the final discrete system equation for the entire problem domain. In Eq. (34), Φ_i is matrix of RPIM shape functions, which are defined with respect to the type of supports as follow (for simply support):

$$\Phi_i = \begin{bmatrix} \hat{\Phi}_i & 0 & 0 \\ 0 & 0 & 0 \\ 0 & 0 & 0 \end{bmatrix} \tag{39}$$

For clamped support:

$$\Phi_i = \begin{bmatrix} \hat{\Phi}_i & 0 & 0 \\ 0 & \hat{\Phi}_{i,t} & 0 \\ 0 & 0 & \hat{\Phi}_{i,n} \end{bmatrix} \tag{40}$$

$$\hat{\Phi}_{i,n} = n_x \hat{\Phi}_{i,x} + n_y \hat{\Phi}_{i,y} \qquad \hat{\Phi}_{i,t} = n_x \hat{\Phi}_{i,y} - n_y \hat{\Phi}_{i,x} \tag{41}$$

where $\hat{\Phi}_{i,n}$ is shape function of rotation with respect to the axis parallel to the normal direction of the boundary and $\hat{\Phi}_{i,t}$ is shape function rotation with respect to the axis perpendicular to the normal direction of the boundary. The parameters n_x, n_y are the unit outward normal vector on the boundary.

5. Numerical integration

All integrations are over the global problem domain Ω and the global traction boundary Γ_t. In order to evaluate these global integrals, the problem domain is discretized into a set of background cells (See Fig. 4). Hence, a global integration can be expressed as a summation of integrals over these cells. It should be mentioned that in contrast with the FEM, the background cells are required only for integration and any form of cells is acceptable as long as it provides sufficient accuracy in the integrations [5]. The Gauss quadrature scheme that is commonly used in the FEM is employed to perform the integrations numerically over these cells.

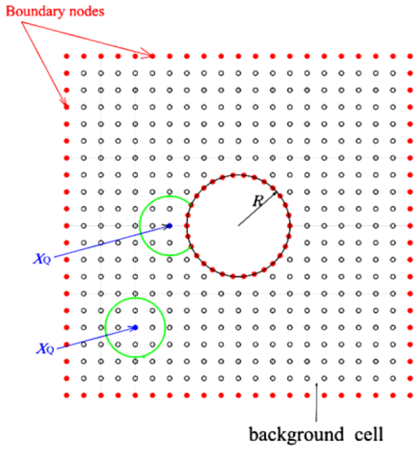

Fig. 4: Meshless model for EFG method with background mesh of cells for integration

6. Numerical experiments and discussions

6.1. Analysis of thick plates without cutout

To validate the proposed method, first a simply supported square thick plate subjected to the following sinusoidal distributed load is analyzed using the proposed method.

$$q(x,y) = q_0 \sin\left(\frac{\pi x}{a}\right)\sin\left(\frac{\pi y}{b}\right) \tag{42}$$

where q_0 is the magnitude of the sinusoidal distributed load at the center of the plate. The mechanical properties of the material are considered as:

$$E = 210\ \text{GPa} \quad \nu = 0.3 \quad G = \frac{E}{2(1+\nu)} \tag{43}$$

The obtained results of maximum transverse displacement and stress components for different thicknesses are presented and compared with the exact and other methods in Table 1. According to this table, obtained results by the presented method are very close to those of refined theories and exact solution. The maximum errors of results for all aspect ratios are acceptable. It should be mentioned that in all figures and tables, the displacements and stresses are presented in the following non-dimensional forms commonly used in the literature:

$$\bar{u}\left(0,\frac{b}{2},\frac{z}{h}\right)=\frac{u.E}{q.h.\xi^{3}};\quad \bar{w}\left(\frac{a}{2},\frac{b}{2},\frac{z}{h}\right)=\frac{100.w.E}{q.h.\xi^{4}};$$
$$\xi=\frac{a}{h}$$
$$\left(\bar{\sigma}_x,\bar{\sigma}_y\right)\left(\frac{a}{2},\frac{b}{2},\frac{z}{h}\right)=\frac{\left(\sigma_x,\sigma_y\right)}{q.\xi^{2}};\tag{44}$$
$$\bar{\tau}_{xy}\left(\frac{a}{2},\frac{b}{2},\frac{z}{h}\right)=\frac{\tau_{xy}}{q.\xi^{2}};$$
$$\bar{\tau}_{xz}\left(0,\frac{b}{2},\frac{z}{h}\right)=\frac{\tau_{xz}}{q.\xi}$$

In this paper for the first time, an estimation function is suggested for calculating the maximum deflection of simply supported thick plates under uniform and sinusoidal transverse loading applied on the top surface of the plate. For this purpose, the full Quadratic method and Rational method [46-48] is applied to obtained results. Using this method, the following equation can be presented to estimate the maximum deflection of the thick plate with respect to the maximum thin plate deflection with an acceptable accuracy.

$$\left[(W_{\max})_P\right]_{TSDT-EFG}^{FSDT-EFG}\cong K_w.(W_{\max})_{CPT}\tag{45}$$

where $(W_{\max})_{CPT}$ is the maximum non-dimensional transverse displacement equivalent plate based on CPT and K_w coefficient for simply supported plate subjected to sinusoidal and uniformly distributed load is given by equations (46) and (47), respectively.

$$K_w=13576.39-181021.742\alpha_1-0.002657\beta_1+45255.43\alpha_1^{2}+(1.3\times10^{-5})\beta_1^{2}+0.000268\alpha_1\beta_1\tag{46}$$

$$K_w=\frac{422278.3636-789530.914901\alpha_1+337979.451995\beta_1}{1-674715.616449\alpha_1+340387.552384\beta_1}\tag{47}$$

In equations (46) and (47) α_1 and β_1 are aspect ratios defined by $\alpha_1=\frac{a}{b}$ and $\beta_1=\frac{b}{h}$. In Table 2, error percentages are calculated using the following equations:

$$\%Error1=\frac{\left[(W_{\max})_P\right]_{TSDT-EFG}^{FSDT-EFG}\text{ - Value by exact solution}}{\text{value by exact solution}}\tag{48}$$

$$\%Error2=\frac{(W_{\text{TSDT-EFG}})_2\text{ - Value by exact solution}}{\text{value by exact solution}}$$

6.2. Analysis of thick plates with cutout

Consider a square plate with different supports, different thicknesses and circular cutout (Radius =1 m) located in arbitrary position subjected to the uniform distributed loading (See Fig. 5). Nodal distribution is 21×21 regular nodes with 14 nodes around the circular cutout. The results obtained for transverse displacement of FSDT & TSDT analysis are showed in Figs. 6-9.

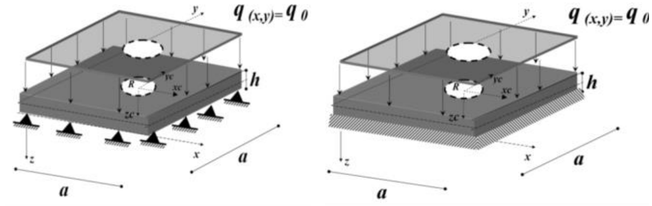

(a) (b)

Fig. 5: Square plate with cutout; (a) Simply Support; (b) Clamped Support

In all graphs, x_c and y_c are the coordinates of the cutout center and the values of α,β,γ are given by:

$$\alpha=\frac{x_c}{a}\qquad \beta=\frac{y_c}{b}\qquad \gamma=\frac{(W_{\max})_{TSDT-EFG}^{FSDT-EFG}}{(W_{\max})_{CPT}}\tag{49}$$

where $(W_{\max})_{CPT}$ is the maximum non-dimensional transverse displacement equivalent plate based on CPT. In Fig. 6, the effect of cutout position on transverse displacement obtained using FSDT theory is examined. Based on these figures it is possible to determine the best position of circular cutout which minimizes the maximum deflection. For simply supported plates, the best position of the cutout is determined as $\alpha=0.5$ and $\beta=0.9$ the value of γ is 1.123. In addition, it can be seen that the maximum value of γ occurs at $\alpha=0.5$ and $\beta=0.6$, which is equal to 1.283. In Fig. 7, the effect of cutout position on transverse displacement obtained using FSDT theory is examined. Based on these figures it is possible to determine the best position of circular cutout, which minimizes the maximum deflection. For clamped supported plate, the best position of the cutout is determined as $\alpha=0.7$ and $\beta=0.75$ the value of γ is equal to 1.421. According to the Fig. 8, at position $\alpha=0.5,0.6,0.8$ and $\beta\cong0.8$, the value of γ is the same ($\gamma=1.141$). In addition, at position $\alpha=0.5,0.6,0.7$ and $\beta=0.835$, the value of γ is the same ($\gamma=1.132$). According to Fig. 8, the best position of the cutout is determined as $\alpha=0.9$ and $\beta=0.6$ the value of γ is equal to 1.16. According to Fig. 9, the best position of the cutout is determined as $\alpha=0.7$ and $\beta=0.76$ the value of γ is equal to 1.572.

Table. 1: Comparison of non-dimensional transverse displacement $\bar{w}$, in-plane normal stress $\bar{\sigma}_{xx}$, in-plane shear stress $\bar{\tau}_{xy}$ and transverse shear stress $\bar{\tau}_{xz}$ of simply supported square plate subjected to sinusoidal distributed load

$\xi = \frac{a}{h}$	Theory	Model	$\bar{w}$	$\bar{\sigma}_{xx}$	$\bar{\sigma}_{xz}$	$\bar{\sigma}_{xy}$
			(0)	(-h/2)	(0)	(-h/2)
10	Present	TSDT-EFG	2.9881	0.2187	0.2547	–
	Ghugal *et al.* [49]	SSNDT	2.9333	0.2125	0.2454	0.1060
	Pagano [50]	Exact	2.9425	0.1988	0.2383	–
	Reddy [42]	TSDT	2.9610	0.1990	0.2380	0.1070
	Ghugal *et al.* [49]	5th OSDT	2.9143	0.1996	0.2383	0.1106
	Reissner [43]	FSDT	2.9340	0.1970	0.1690	0.1060
	Reddy [42]	CPT	2.8020	0.1970	–	0.1060
20	Present	TSDT-EFG	2.9402	0.2104	0.2415	–
	Pagano [50]	Exact	2.8377	0.1979	0.2386	–
	Ghugal *et al.* [49]	5th OSDT	2.8303	0.1981	0.2386	0.1074
50	Present	TSDT-EFG	2.8020	0.1967	0.2312	–
	Ghugal *et al.* [49]	SSNDT	2.7991	0.2100	0.2456	0.1060
	Pagano [50]	Exact	2.8082	0.1976	0.2386	–
	Ghugal *et al.* [49]	5th OSDT	2.8070	0.1977	0.2387	0.1066
100	Present	TSDT-EFG	2.7660	0.1948	0.2310	–
	Ghugal *et al.* [49]	SSNDT	2.7949	0.2099	0.2456	0.1060
	Pagano [50]	Exact	2.8040	0.1976	0.2387	–
	Ghugal *et al.* [49]	5th OSDT	2.8037	0.1976	0.2387	0.1064

Table. 2: K_w coefficient for simply supported plate subjected to sinusoidal distributed load

α_1	β_1	K_w	$(w_{max})_{CPT}$ Reddy (1990)	TSDT-EFG *	TSDT-EFG**	Exact Reddy (1990)
				Error1	Error2	
1	10	1.0660	2.803	2.985	2.988	2.9610
				0.83%	0.92%	
	20	1.0460		2.929	2.934	2.8377
				3.23%	3.39%	
	50	1.0017		2.805	2.796	2.8082
				0.11%	0.11%	
	100	0.9797		2.744	2.757	2.8040
				2.16%	1.68%	
3	10	1.0386	9.080	9.407	9.448	9.4790
				0.76%	0.33%	
	20	1.0239		9.274	9.188	9.2810
				0.07%	1.00%	
	50	0.9956		9.017	9.090	9.1170
				1.09%	0.30%	
	100	1.0005		9.061	9.081	9.0810
				0.22%	0.00%	

**Maximum deflection of a thick plate for simply supported with Estimate function Proposed* $\left[(W_{max})_P\right]_{TSDT-EFG}$

*** Maximum deflection of a thick plate for simply support present theory* $(W_{TSDT-EFG})_2$

Table. 3: K_w coefficient for simply and clamped supported plate with cutout subjected to sinusoidal and uniform distributed load distributed load

$$K_w = \xi_1 + \xi_2\alpha + \xi_3\beta + \xi_4\alpha^2 + \xi_5\beta^2 + \xi_6\alpha^3 + \xi_7\beta^3 + \xi_8\alpha\beta + \xi_9\alpha^2\beta + \xi_{10}\alpha\beta^2$$

b/h	Type	$(W_{max})_{CPT}$* [36]	Coefficients										$(W_{max})_{TSDT-EFG} \cong K_w.(W_{max})_{CPT}$
			ξ_1	ξ_2	ξ_3	ξ_4	ξ_5	ξ_6	ξ_7	ξ_8	ξ_9	ξ_{10}	
10	FSDT	4.444	-2.3521	9.059	8.626	-11.25	-10.73	4.433	4.324	-5.8	2.71	2.411	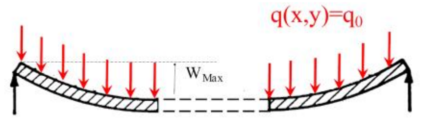 Cutout radius =1m Square plate (a = b = 10 m) All Edge is Simply Support Load type is disterbution uniform load(q_0) $\alpha = x_c/a \quad \beta = y_c/b$
20			-2.4468	9.465	8.289	-12.16	-10.59	4.903	4.398	-5.266	2.663	2.108	
50			-2.4556	9.099	8.423	-11.91	-11.05	4.903	4.678	-4.703	2.386	1.961	
100			-2.4276	8.842	8.462	-11.68	-11.23	4.847	4.787	-4.418	2.236	1.893	
10	TSDT		-2.3933	9.905	8.164	-12.4	-10.05	4.879	4.064	-5.905	2.944	2.251	
20			-2.4278	9.525	8.225	-12.19	-10.46	4.897	4.323	-5.349	2.708	2.123	
50			-2.4433	9.117	8.384	-11.91	-10.97	4.887	4.63	-4.759	2.415	1.975	
100			-2.4331	8.967	8.383	-11.84	-11.11	4.908	4.738	-4.45	2.28	1.876	
10	FSDT	1.375	-3.3884	12.26	11.78	-19.29	-18.88	9.254	9.496	0.552	0.486	-0.442	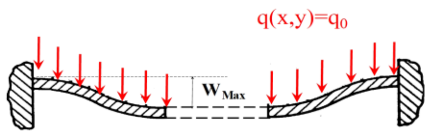 Cutout radius =1m Square plate (a = b = 10 m) All Edge is Clamped Support Load type is disterbution uniform load(q_0) $\alpha = x_c/a \quad \beta = y_c/b$
20			-1.811	7.627	7.13	-14.49	-13.88	7.681	7.522	4.949	-1.56	-1.807	
50			-0.8824	4.97	4.802	-12.06	-11.87	6.971	6.863	8.02	-2.878	-2.762	
100			-0.6612	4.303	4.327	-11.42	-11.48	6.74	6.742	8.708	-3.115	-3	
10	TSDT		-3.9902	14.06	13.54	-21.12	-20.75	9.845	10.22	-1.101	1.254	0.068	
20			-2.1129	8.509	7.962	-15.37	-14.72	7.959	7.829	4.054	-1.154	-1.525	
50			-0.9867	5.274	5.044	-12.32	-12.05	7.043	6.915	7.644	-2.72	-2.649	
100			-0.7028	4.49	4.355	-11.65	-11.49	6.836	6.745	8.616	-3.075	-2.978	
10	FSDT	2.803	-1.8408	7.624	7.03	-8.798	-8.056	3.296	3.107	-5.75	2.561	2.198	
20			-1.8048	7.704	6.502	-9.504	-7.905	3.745	3.224	-4.747	2.327	1.766	
50			-1.7282	7.138	6.486	-9.129	-8.294	3.726	3.497	-3.911	1.935	1.548	
100			-1.6891	6.891	6.475	-8.945	-8.436	3.704	3.594	-3.565	1.76	1.465	

10	TSDT		-1.7536	7.744	6.467	-9.666	-7.933	3.864	3.245	-4.089	1.991	1.512	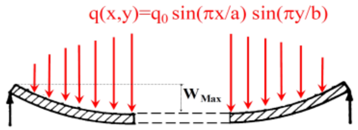 Cutout radius =1m Square plate (a = b = 10 m) All Edge is Simply Support Load type is disterbution Sinusoidal load q0.sin(px/a) sin(py/b) $\alpha = x_c/a \quad \beta = y_c/b$
20			-1.493	6.885	5.838	-9.029	-7.617	3.724	3.235	-3.171	1.672	1.246	
50			-1.3767	6.405	5.505	-8.685	-7.479	3.677	3.271	-2.489	1.402	1.008	
100			-1.3587	6.316	5.4	-8.684	-7.457	3.716	3.304	-2.193	1.29	0.89	
10	FSDT	0.628	-4.3529	15.79	15.56	-23.81	-23.78	11.55	11.7	0	0	0	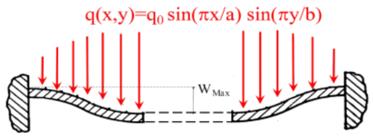 Cutout radius =1m Square plate (a = b = 10 m) All Edge is Clapmed Support Load type is disterbution Sinusoidal load q0.sin(px/a) sin(py/b) $\alpha = x_c/a \quad \beta = y_c/b$
20			-2.5878	10.56	10.05	-18.55	-17.96	9.731	9.598	5.025	-1.796	-2.045	
50			-1.1033	6.353	6.518	-15.09	-15.41	8.855	8.973	10.5	-4.03	-3.798	
100			-0.7662	5.312	5.84	-14.08	-14.89	8.483	8.823	11.52	-4.371	-4.151	
10	TSDT		-4.5301	16.74	16.46	-25.12	-25.11	12.13	12.31	0	0	0	
20			-3.122	12.04	11.41	-19.83	-19.09	10.08	9.939	3.24	-1.055	-1.468	
50			-1.2675	6.837	6.878	-15.47	-15.63	8.949	9.01	9.849	-3.765	-3.596	
100			-0.8209	5.509	5.924	-14.32	-14.98	8.597	8.859	11.43	-4.356	-4.114	

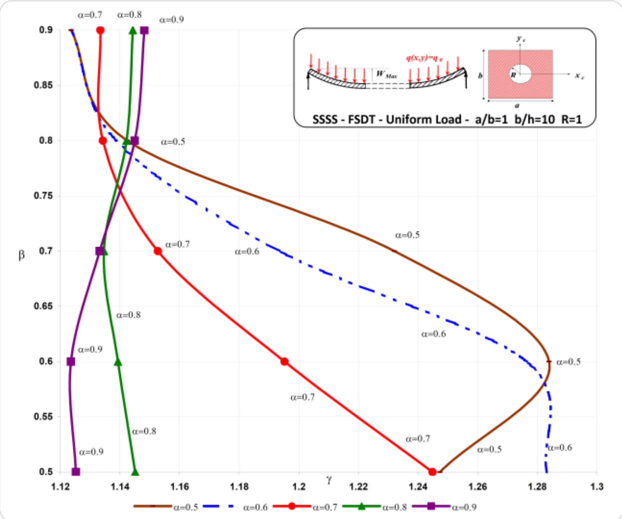

Fig. 6: Relation of α, β, γ- simply supported Plate subjected to uniform distributed load ratio - b/h=10 (FSDT)

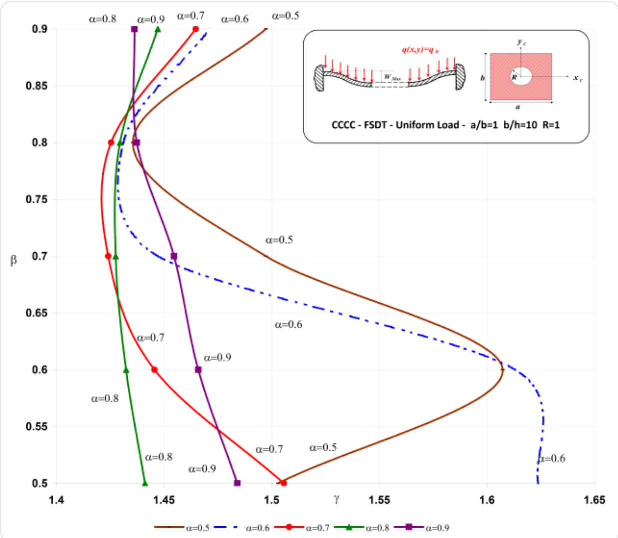

Fig. 7: Relation of α, β, γ- clamped supported Plate subjected to uniform distributed load ratio - b/h=10 (FSDT)

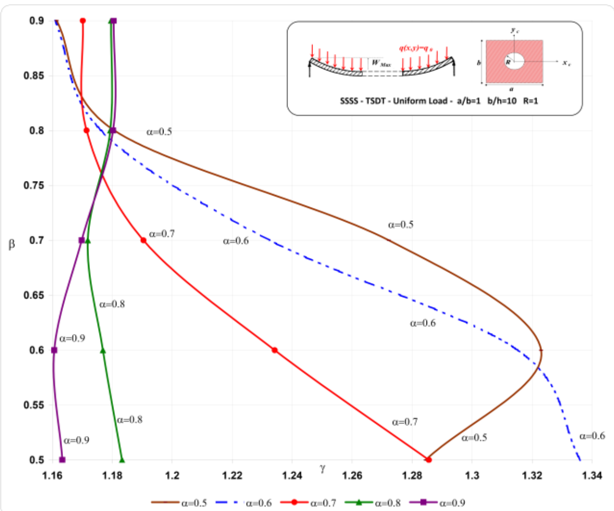

Fig. 8: Relation of α, β, γ - simply supported Plate subjected to uniform distributed load ratio - b/h=10 (TSDT)

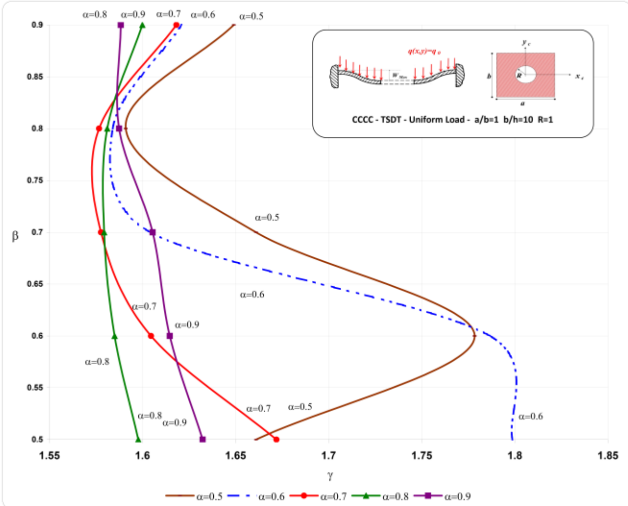

Fig. 9: Relation of α, β, γ - clamped supported Plate subjected to uniform distributed load ratio - b/h=10 (TSDT)

Here again, a new relation has been proposed to determine transverse displacement of plates with cutout based on FSDT & TSDT theories. The estimation function obtained by the full cubic method, is the same as introduced in Eq. (45) except that the K_w coefficient for a simply supported thick plate with cutout subjected to uniform and sinusoidal distributed loadings are defined by:

$$K_w = \xi_1 + \xi_2\alpha + \xi_3\beta + \xi_4\alpha^2 + \xi_5\beta^2 + \xi_6\alpha^3 + \xi_7\beta^3 + \xi_8\alpha\beta + \xi_9\alpha^2\beta + \xi_{10}\alpha\beta^2 \tag{50}$$

where $\xi_1,..., \xi_{10}$ are constant values which are different for uniform and sinusoidal loading and listed in the Table 3.

$$Average\,Error = \frac{\left|(W_{\max})_P\right|_{TSDT-EFG}^{FSDT-EFG} - (W_{\max})_{TSDT-EFG}^{FSDT-EFG}}{(W_{\max})_{CPT}} \tag{51}$$

where $\left|(W_{\max})_P\right|_{TSDT-EFG}^{FSDT-EFG}$ is the maximum deflection of the thick plate obtained by the proposed estimation function. The diagrams of obtained results by FSDT and TSDT theory are compared with the results of estimation functions in Figs. 10 and 11, respectively. According to these figures, it can be seen that the estimation functions have a good agreement with the numerical results.

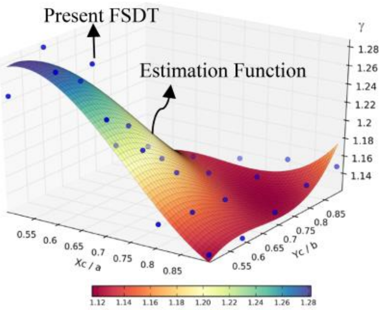

Fig. 10: Comparison between the estimation function and FSDT results for simply supported plate subjected to uniform load and b/h=10

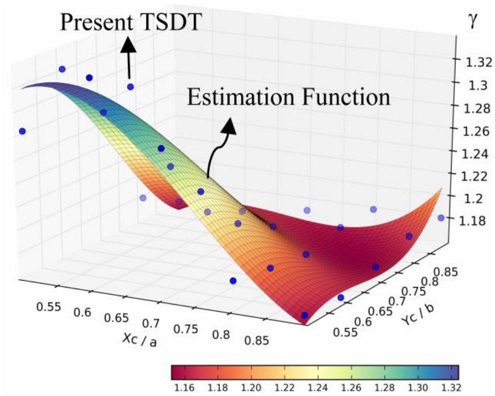

Fig. 11: Comparison between the estimation function and TSDT results for simply supported plate subjected to uniform load and b/h=10

7. Conclusions

In this paper, the EFG method has been developed for analysis of thick plates with and without cutout. The formulations have been tested for different supports, aspect ratios and cutout coordinates. According to the results obtained by the present method, the full cubic function is proposed to estimate the maximum deflection of thick plates. The obtained results have been compared with published solutions and excellent agreement is seen. The main results of this paper can be outlined as follows:

- By choosing the appropriate shape functions for the deflection and rotations, the presented EFG method has successfully overcome the shear-locking problem.
- The proposed model is insensitive to node distribution in two directions. Additionally, the nodes can be either regularly or irregularly distributed. It should be mentioned that, using irregularly distributed nodes is unavoidable for modeling of plates with cutout.
- Based on obtained results and cubic polynomial method, the estimation functions for predicting maximum deflection of plates with and without cutout have been presented.
- For various boundary conditions and loadings, the obtained results using the presented EFG method and estimation functions have a good agreement with those obtained by refined theories and exact solution.

The effect of cutout position on maximum deflection has been investigated using various diagrams and tables. The best position of circular cutout, in which the deflection is minimum, is determined experimentally.

References:

[1] M.A. Puso, J.S. Chen, E. Zywicz, W. Elmer. Meshfree and finite element nodal integration methods, International Journal for Numerical Methods in Engineering. 74 (2008) 416-446.

[2] G.R. Liu. Meshfree methods: moving beyond the finite element method, Taylor & Francis, 2009.

[3] G.R. Liu, Y.T. Gu. An introduction to meshfree methods and their programming. Springer Science & Business Media, 2005.

[4] V.M. Sreehari, D.K. Maiti. Buckling and post buckling characteristics of laminated composite plates with damage under thermo-mechanical loading. In Structures. 6 (2016) 9-19.

[5] G.R. Liu, G.Y. Zhang, Y. Gu, Y.Y. Wang. A meshfree radial point interpolation method (RPIM) for three-dimensional solids. Computational Mechanics, 36 (2005) 421-430.

[6] A. Hussain, Y.P. Liu, S.L. Chan. Finite element modeling and design of single angle member under bi-axial bending, In Structures. 16 (2018) 373-389.

[7] J. Akl, F. Alladkani, P. Dumond. Comparing and optimizing analytical, numerical and experimental vibration models for a simply-supported ribbed plate, In Structures. 23 (2002) 690-701.

[8] D.L. Christy, T.M. Pillai, P. Nagarajan. Thin plate element for applied element method, In Structures. 22 (2019) 1-12.

[9] T. Liszka, J. Orkisz. The finite difference method at arbitrary irregular grids and its application in applied mechanics. Computers & Structures, 11 (1980) 83-95.

[10] L.B. Lucy. A numerical approach to the testing of the fission hypothesis, The astronomical journal, 82 (1977) 1013-1024.

[11] N. R. Aluru, A point collocation method based on reproducing kernel approximations, International Journal for Numerical Methods in Engineering, 47 (2000) 1083-1121.

[12] T. Belytschko, Y.Y. Lu, L. Gu, Element-free Galerkin methods, International journal for numerical methods in engineering, 37 (1994) 229-256.

[13] J.S. Chen, D. Wang, A constrained reproducing kernel particle formulation for shear deformable shell in Cartesian coordinates, International Journal for Numerical Methods in Engineering, 68 (2006) 151-172.

[14] S. Tanaka, H. Suzuki, S. Sadamoto, M. Imachi, T.Q. Bui, Analysis of cracked shear deformable plates by an effective meshfree plate formulation, Engineering Fracture Mechanics. 144 (2015) 142-157.

[15] S.N. Atluri, T. Zhu, A new meshless local Petrov-Galerkin (MLPG) approach in computational mechanics, Computational mechanics, 22 (1998) 117-127.

[16] G.R. Liu, Y.T. Gu, A local radial point interpolation method (LRPIM) for free vibration analyses of 2-D solids, Journal of Sound and vibration, 246 (2001) 29-46.

[17] G.R. Liu, Y.T. Gu, A local point interpolation method for stress analysis of two-dimensional solids, Structural Engineering and Mechanics, 11 (2001) 221-236.

[18] L. Gu, Moving kriging interpolation and element-free Galerkin method, International journal for numerical methods in engineering, 56 (2003) 1-11.

[19] Y.T. Gu, G. R. Liu, A boundary radial point interpolation method (BRPIM) for 2-D structural analyses, Structural engineering and mechanics, 15 (2003) 535-550.

[20] G.R. Liu, Y.L. Wu, H. Ding, Meshfree weak–strong (MWS) form method and its application to incompressible flow problems, International journal for numerical methods in fluids, 46 (2004) 1025-1047.

[21] J. Chen, W. Tang, P. Huang, L. Xu, A mesh-free analysis method of structural elements of engineering structures based on B-spline wavelet basis function, Structural Engineering and Mechanics, 57 (2016) 281-294.

[22] S. Beissel, T. Belytschko, Nodal integration of the element-free Galerkin method, Computer methods in applied mechanics and engineering, 139 (1996) 49-74.

[23] G.R. Liu, L. Yan, J.G. Wang, Y.T. Gu, Point interpolation method based on local residual formulation using radial basis functions. Structural Engineering and Mechanics, 14 (2002) 713-732.

[24] T. Most, C. Bucher, A moving least squares weighting function for the element-free Galerkin method which almost fulfills essential boundary conditions, Structural Engineering and Mechanics, 21 (2005) 315-332.

[25] Y. Liu, T. Belytschko, A new support integration scheme for the weak form in mesh-free methods, International journal for numerical methods in engineering, 82 (2010) 699-715.

[26] J.S. Chen, C.T. Wu, S. Yoon, Y. You, A stabilized conforming nodal integration for Galerkin mesh-free methods, International journal for numerical methods in engineering, 50 (2001) 435-466.

[27] J. Sladek, V. Sladek, H. A. Mang, Meshless formulations for simply supported and clamped plate problems, International Journal for Numerical Methods in Engineering, 55 (2002) 359-375.

[28] J. Alihemmati, Y.T. Beni, Developing three-dimensional mesh-free Galerkin method for structural analysis of general polygonal geometries, Engineering with Computers, 1 (2019) 1-10.

[29] Y. Cao, L. Yao, Y. Yin, New treatment of essential boundary conditions in EFG method by coupling with RPIM, Acta Mechanica Solida Sinica, 26 (2013) 302-316.

[30] Y. Choi, S. Kim, Analysis of Mindlin plate by the element free Galerkin method applying penalty technique, In 40th Structures, Structural Dynamics, and Materials Conference and Exhibit, 1999.

[31] B.M. Donning, W.K. Liu, Meshless methods for shear-deformable beams and plates, Computer Methods in Applied Mechanics and Engineering, 152 (1998) 47-71.

[32] V. Gulizzi, I. Benedetti, A. Milazzo, An implicit mesh discontinuous Galerkin formulation for higher-order plate theories, Mechanics of Advanced Materials and Structures, 1 (2019) 1-15.

[33] M. Khezri, M. Gharib, K.J.R. Rasmussen, A unified approach to meshless analysis of thin to moderately thick plates based on a shear-locking-free Mindlin theory formulation, Thin-Walled Structures, 124 (2018) 161-179.

[34] D.H. Konda, J.A.F. Santiago, J.C.F. Telles, J.P.F. Mello, E.G.A. Costa, A meshless Reissner plate bending procedure using local radial point interpolation with an efficient integration scheme, Engineering Analysis with Boundary Elements, 99 (2019) 46-59.

[35] Y. Li, G.R. Liu, An element-free smoothed radial point interpolation method (EFS-RPIM) for 2D and 3D solid mechanics problems, Computers & Mathematics with Applications, 77 (2019) 441-465.

[36] X. Liu, G.R. Liu, J. Wang, Y. Zhou, A wavelet multiresolution interpolation Galerkin method for targeted local solution enrichment, Computational Mechanics, 64 (2019) 989-1016.

[37] M.H.G. Rad, F. Shahabian, S.M. Hosseini, A meshless local Petrov–Galerkin method for nonlinear dynamic analyses of hyper-elastic FG thick hollow cylinder with Rayleigh damping, Acta Mechanica, 226 (2015) 1497-1513.

[38] C.H. Thai, H. Nguyen-Xuan, A moving kriging interpolation meshfree method based on naturally stabilized nodal integration scheme for plate analysis, International Journal of Computational Methods, 16 (2019) 1850100.

[39] Thai, H. T., & Choi, D. H. (2013). Analytical solutions of refined plate theory for bending, buckling and vibration analyses of thick plates. Applied Mathematical Modelling, 37(18-19), 8310-8323.

[40] A.C.A. Ferreira, P.M.V. Ribeiro, Reduced-order strategy for meshless solution of plate bending problems with the generalized finite difference method, Latin American Journal of Solids and Structures, 16 (2019) e140.

[41] Tash, F. Y., & Neya, B. N. (2020). An analytical solution for bending of transversely isotropic thick rectangular plates with variable thickness. Applied Mathematical Modelling, 77, 1582-1602.

[42] J.N. Reddy, Theory and analysis of elastic plates and shells. CRC press. 1999.

[43] E. Reissner, On the theory of transverse bending of elastic plates, International Journal of Solids and Structures, 12 (1976) 545-554.

[44] Dorduncu, M., Kaya, K., & Ergin, O. F. (2020). Peridynamic Analysis of Laminated Composite Plates Based on First-Order Shear Deformation Theory. International Journal of Applied Mechanics, 2050031.

[45] Cui, X. Y., Liu, G. R., & Li, G. Y. (2010). Analysis of Mindlin–Reissner plates using cell-based smoothed radial point interpolation method. International Journal of Applied Mechanics, 2(03), 653-680.

[46] M. Hu, X. Shi, T. Wang, F. Liu, A note on cubic polynomial interpolation, Computers & Mathematics with Applications, 56 (2008) 1358-1363.

[47] E. Meijering, M. Unser, A note on cubic convolution interpolation, IEEE Transactions on Image processing, 12 (2003) 477-479.

[48] M.H. Kharrazi, Rational method for analysis and design of steel plate walls. Ph.D. Dssertation, University of British Columbia, Canada, 2005.

[49] Ghugal, Y. M., & Sayyad, A. S. (2013). Stress analysis of thick laminated plates using trigonometric shear deformation theory. International Journal of Applied Mechanics, 5(01), 1350003.

[50] N.J. Pagano, Exact solutions for rectangular bidirectional composites and sandwich plates, Journal of composite materials, 4 (1970) 20-34.

Appendix A: Stiffness Coefficients

$$
\begin{aligned}
\hat{\Phi}_{i,x} &= \frac{\partial \Phi}{\partial x} = \sum_{i=1}^{n} \frac{\partial R_i}{\partial x} = 2q\left(r_i^2 + c^2\right)^{q-1}(x - x_i) \\
\hat{\Phi}_{i,y} &= \frac{\partial \Phi}{\partial y} = \sum_{i=1}^{n} \frac{\partial R_i}{\partial y} = 2q\left(r_i^2 + c^2\right)^{q-1}(y - y_i) \\
\hat{\Phi}_{i,xx} &= \frac{\partial^2 \Phi}{\partial x^2} = \sum_{i=1}^{n} \frac{\partial^2 R_i}{\partial x^2} = 2q\left(r_i^2 + c^2\right)^{q-1} + 4q(q-1)\left(r_i^2 + c^2\right)^{q-2}(x - x_i)^2 \\
\hat{\Phi}_{i,yy} &= \frac{\partial^2 \Phi}{\partial y^2} = \sum_{i=1}^{n} \frac{\partial^2 R_i}{\partial y^2} = 2q\left(r_i^2 + c^2\right)^{q-1} + 4q(q-1)\left(r_i^2 + c^2\right)^{q-2}(y - y_i)^2 \\
\hat{\Phi}_{i,xy} &= \frac{\partial^2 \Phi}{\partial xy} = \sum_{i=1}^{n} \frac{\partial^2 R_i}{\partial xy} = 4q(q-1)\left(r_i^2 + c^2\right)^{q-2}(x - x_i)(y - y_i)
\end{aligned}
\tag{A1}
$$

Appendix B: Stiffness Coefficients

$$
\Delta = \begin{bmatrix}
1 & \nu & 0 & 0 & 0 \\
\nu & 1 & 0 & 0 & 0 \\
0 & 0 & \frac{1-\nu}{2} & 0 & 0 \\
0 & 0 & 0 & \Theta.\frac{1-\nu}{2} & 0 \\
0 & 0 & 0 & 0 & \Theta.\frac{1-\nu}{2}
\end{bmatrix}, \quad \Delta_{11} = \Delta_{(1,1)}
\tag{B1}
$$

$$
[K(1,2),(2,1)]_{ij} = \frac{Eh}{(6720(1-\nu^2))}
\begin{bmatrix}
30\chi^2 h^6 G\hat{\phi}_{i,xx}\hat{\phi}_{j,yy} + 15\chi^2 h^6\left(\Delta_{11}\hat{\phi}_{i,xx}\hat{\phi}_{j,xx} + \Delta_{12}\hat{\phi}_{i,yy}\hat{\phi}_{j,xx}\right) - \ldots \\
168\chi G h^4\hat{\phi}_{i,xy}\hat{\phi}_{j,xy} - 84\chi h^4\left(\Delta_{11}\hat{\phi}_{i,xx}\hat{\phi}_{j,xx} + \Delta_{12}\hat{\phi}_{i,yy}\hat{\phi}_{j,xx}\right) + \ldots \\
84\eta^2\Theta G h^4\hat{\phi}_{i,x}\hat{\phi}_{j,x} - 1120\eta\Theta G h^2\hat{\phi}_{i,x}\hat{\phi}_{j,x} + 6270\Theta G\hat{\phi}_{i,x}\hat{\phi}_{j,x}
\end{bmatrix}
\tag{B2}
$$

$$
[K(1,3),(3,1)]_{ij} = \frac{Eh}{(6720(1-\nu^2))}
\begin{bmatrix}
30\chi^2 h^6 G.\hat{\phi}_{i,xy}\hat{\phi}_{j,xy} + 15\chi^2 h^6\left(\Delta_{12}\hat{\phi}_{i,xx}\hat{\phi}_{j,yy} + \Delta_{11}\hat{\phi}_{i,yy}\hat{\phi}_{j,yy}\right) - \ldots \\
168\chi G h^4\hat{\phi}_{i,xy}\hat{\phi}_{j,xy} - 84\chi h^4\left(\Delta_{12}\hat{\phi}_{i,xx}\hat{\phi}_{j,yy} + \Delta_{11}\hat{\phi}_{i,yy}\hat{\phi}_{j,yy}\right) + \ldots \\
84\eta^2\Theta G h^4\hat{\phi}_{i,y}\hat{\phi}_{j,y} - 1120\eta\Theta G h^2\hat{\phi}_{i,y}\hat{\phi}_{j,y} + 6270\Theta G\hat{\phi}_{i,x}\hat{\phi}_{j,x}
\end{bmatrix}
\tag{B3}
$$

$$
[K(2,2)]_{ij} = \frac{Eh}{(6720(1-\nu^2))}
\begin{bmatrix}
15\chi^2 h^6\left(G\hat{\phi}_{i,y}\hat{\phi}_{j,xy} + \Delta_{11}\hat{\phi}_{i,xx}\hat{\phi}_{j,xx}\right) - 168\chi h^4\left(\Delta_{11}\hat{\phi}_{i,xx}\hat{\phi}_{j,xx} + G\hat{\phi}_{i,xy}\hat{\phi}_{j,xy}\right) + \ldots \\
84\eta^2\Theta G h^4\hat{\phi}_{i,x}\hat{\phi}_{j,x} + 560h^2\left(\Delta_{11}\hat{\phi}_{i,xx}\hat{\phi}_{j,xx} + G\hat{\phi}_{i,xy}\hat{\phi}_{j,xy}\right) - \ldots \\
1120\eta\Theta G h^2\hat{\phi}_{i,x}\hat{\phi}_{j,x} + 6270\Theta G\hat{\phi}_{i,x}\hat{\phi}_{j,x}
\end{bmatrix}
\tag{B4}
$$

$$
[K(2,3),(3,2)]_{ij} = \frac{Eh}{(6720(1-\nu^2))} h^2\left[15\Omega^2 h^4 - 168\chi h^2 + 560\right]\left[\Delta_{12}\hat{\phi}_{i,xx}\hat{\phi}_{j,yy} + G\hat{\phi}_{i,xy}\hat{\phi}_{j,xy}\right]
\tag{B5}
$$

$$
[K(3,3)]_{ij} = \frac{Eh}{(6720(1-\nu^2))}.
\begin{bmatrix}
15\chi^2 h^6\left(G\hat{\phi}_{i,xy}\hat{\phi}_{j,xy} + \Delta_{11}\hat{\phi}_{i,yy}\hat{\phi}_{j,yy}\right) - 168\chi h^4\left(\Delta_{11}\hat{\phi}_{i,yy}\hat{\phi}_{j,yy} + G\hat{\phi}_{i,xy}\hat{\phi}_{j,xy}\right) + \ldots. \\
84\eta^2\Theta G h^4\hat{\phi}_{i,y}\hat{\phi}_{j,y} + 560h^2\left(\Delta_{11}\hat{\phi}_{i,yy}\hat{\phi}_{j,yy} + G\hat{\phi}_{i,xy}\hat{\phi}_{j,xy}\right) - \ldots. \\
-1120\Theta G\left(\eta h^2 - 6\right)\hat{\phi}_{i,y}\hat{\phi}_{j,y}
\end{bmatrix}
\tag{B6}
$$